This is a non-final version of an article published in final form in Neuro Oncol. 2021 Jan 30;23(1):88-99. doi: 10.1093/neuonc/noaa151

Cisplatin-induced peripheral neuropathy is associated to neuronal senescence-like response

Aina Calls[1,2], Abel Torres-Espin[3], Xavier Navarro[1,2], Victor Yuste[4], Esther Udina[1,2]*, Jordi Bruna[1,2,4]*

[1]Department of Cell Biology, Physiology and Immunology; Institute of Neuroscience, Universitat Autònoma de Barcelona, Bellaterra, Spain.

[2]Centro de Investigación Biomédica en Red sobre Enfermedades Neurodegenerativas (CIBERNED), Bellaterra, Spain.

[3]Department of Neurological Surgery, University of California, Brain and Spinal Injury Center (BRAIN), San Francisco, United States of America.

[4]Department of Biochemistry; Institute of Neuroscience, Universitat Autònoma de Barcelona, Bellaterra, Spain.

[5]Unit of Neuro-Oncology, Hospital Universitari de Bellvitge-ICO L'Hospitalet, IDIBELL, Hospitalet, Spain.

Corresponding author: Jordi Bruna MD, PhD (35078jbe@comb.cat)

Unit of Neuro-Oncology, Hospital Universitari de Bellvitge-ICO L'Hospitalet, IDIBELL, Hospitalet, Spain.

*EU and JB contributed as co-senior autors

The authors have declared that no conflict of interest exist

Abstract

Cisplatin-Induced Peripheral Neuropathy (CIPN) is a frequent serious dose-limiting adverse event that often causes cancer treatment reduction or even cessation. The exact pathophysiology of CIPN is poorly understood, so the chance of developing neuroprotective treatment is reduced. In this study, we aimed to determine the exact mechanisms involved in CIPN development. To this end, we have analysed the changes in the transcriptome profile of DRG sensory neurons from a well characterized neurophysiological mice model of CIPN by single-cell RNA sequencing (scRNAseq). Gene Ontology analysis of the scRNAseq data indicated that cisplatin treatment induces the up regulation of biological pathways related with DNA damage response (DDR). Moreover, DRG neurons also upregulated the *Cdkn1a* gene, which is confirmed by the measurement of its protein product p21. However, neither apoptosis activation pathways or apoptotic phenotype was observed in DRG sensory neurons of cisplatin-treated mice. In contrast, these neurons expressed several senescence hallmarks, including senescence-associated beta-galactosidase, phospho-H2AX and nuclear Nfkb-p65 proteins. We conclude that after cisplatin-induced DNA damage, p21 appears as the most relevant downstream factor of the DDR in DRG sensory neurons. As a consequence, sensory neurons survive in a non-functional senescence-like state.

Introduction

Chemotherapy-induced peripheral neuropathy (CIPN) is a well-known and unresolved adverse event of drugs widely used to treat prevalent cancers (1). The development of CIPN is dose-limiting and can lead to treatment withdrawal. As a consequence, CIPN has a direct impact on patients' survival and quality of life due to its long-lasting nature (2–4). Moreover, the management of patients with CIPN imposes a relevant economic burden for health Systems (5).

Among neurotoxic cytostatic drugs causing CIPN, platinum compounds are one of the most widely used. Despite the successful emergence of new approaches to cancer treatment such as immune checkpoint inhibitors (6), platinum drugs are still the cornerstone treatment in several clinical settings for high prevalent tumours, both in children and in adulthood (7). Cisplatin, the most common platinum drug, induces a progressive pure sensory neuropathy in a typical sock-and-glove distribution. Symptomatology ranges from mild-moderate decreased vibratory sensitivity, numbness and paresthesias to more severe symptoms that eventually result in disabling self-care and ataxic gait (7,8).

Prevention or treatment of platinum-induced peripheral neuropathy are still unmet clinical needs (9,10). A major reason for this lack of effective treatments is the incomplete knowledge of the pathogenesis of this peripheral neuropathy pathogenesis. Data from neoplastic cells indicates that cisplatin-induced genotoxic lesions (formation of platinum DNA adducts) and increased levels of oxidative stress are the main mechanisms in inhibiting cell division (11). On the other hand, initial observations on the peripheral nervous system showed a correlation between the severity of neuropathy and the amount of platinum in the patients dorsal root ganglia (DRG) cells (12). Since then, preclinical studies have

attempted to elucidate the mechanisms underlying this primary sensory neuropathy. A constellation of multiple effector molecular pathways leading to DRG neuron death has been studied. Defects on nuclear and mitochondrial DNA platinum adducts repair, as well as the increase of oxidative cellular stress leading to apoptosis are the main factors reported in *in vitro* experiments. However, mechanisms of neuronal death by apoptosis in animal models of cisplatin-induced neuropathy are poorly supported (13,14). In addition, these animal models did not show correspondence between their well-established nerve conduction alterations and the loss of nerve fibers. Notwithstanding, other processes have also been entailed, including phosphoinositide 3 kinase dysregulations and alterations in ion channel and calcium signalling (revised in Calls et al., 2020). In any case, an integrative functional network encompassing the more relevant findings is still missing. This fact and the incomplete knowledge of pathogenic factors, may explain the unsuccessful transfer from preclinical results to therapeutic clinical trials (9).

Therefore, we sought to further decipher the neuropathogenic mechanisms underlying cisplatin neurotoxicity in a well characterized mouse model of cisplatin-induced neuropathy that closely mimics the clinical features observed in patients. We performed a single-cell RNA sequencing (scRNAseq) of isolated DRG cells from treated mice, followed by molecular and morphological analysis. The results show that the most relevant up-regulated gene in neurons in the cisplatin treated mice was *Cdkn1a*. The significance of this finding was later corroborated by assessing p21 protein levels. p21 has multiple divergent roles depending on the nature of the cellular stresses, including apoptosis modulation, senescence induction, or cellular quiescence status maintenance (15). The fact that cell-cycle arrest is not needed to induce apoptosis in differentiated neurons, opened the hypothesis of senescence involvement as response to the chronic platinum-DNA adduct damage in

neurons. To further explore this assumption, we checked the most accepted morphological and molecular hallmarks of cell senescence in our animal model (16). In addition, we explored key features of apoptosis activation. Altogether, our data indicate that neurons exposed to cisplatin, in response to the suffered DNA damage, activate p21 and survive in a senescence-like phenotype with an impaired functional status.

Results

Cisplatin-treated mice develop a painful peripheral sensory neuropathy. The cisplatin administration schedule was planned to give 7 mg/Kg cisplatin once a week until reaching a total cumulated dose (TCD) of 42mg/kg. This dose is equivalent to human doses in which neuropathy starts developing, according to published allometric dose translations (8,17). However, mice treated with such cisplatin dosage experienced a weight loss ≥ 10% after the second cisplatin administration. Therefore, the cisplatin dose was modified and reduced to a half (3.5 mg/Kg) once a week. Thus, the planned TCD was achieved at 9w. During the coasting effect evaluation-time (from 10 to 16w) animals recovered their body weight similar to baseline values (Figure 1A).

First, we characterized our model of cisplatin-induced neuropathy. Mice treated with cisplatin experienced a significant progressive decrease in the amplitudes of sensory nerve action potentials (SNAP) recordered in the digital nerves (Figure 1B). Similarly, the mixed sensory-motor compound nerve action potential (CNAP) recorded in the proximal and distal caudal nerves also experienced a significant progressive decrease over time in treated group (Figure 1, C and D). The decrease in the digital and caudal NAPs started at 10w of study and gradually worsened over time, with a maximum negative peak at 16w of follow-up. In contrast, the amplitude of the compound muscle action potentials (CMAP) recorded at the plantar muscle in cisplatin-treated mice was maintained equivalent to control mice (Figure 1E). In the algesimetry test, cisplatin-treated animals had a significantly reduced withdrawal thresholds to mechanical stimulation applied to the plantar paw, indicative of hyperalgesia. This increased response to mechanical stimuli reached a peak at 9w and tended to recover to basal values during the coasting effect follow-up period (Figure 1F).

These functional findings are in accordance with those reported in patients with cisplatin-induced neuropaty (8,18).

The number and density of myelinated axons in semithin cross- sections of the sciatic and tibial nerves did not differ between control and cisplatin-treated mice at the different evaluation time points evaluated (Figure 1, G and H). Likewise, intraepidermal nerve fiber density (IENFD) in the hindpaw pad did not show differences between control and cisplatin-treated animals when labeling fibers with the pan-neuronal marker protein gene product 9.5 (PGP9.5) (Figure 1I). However, labeling against the peptidergic neuron marker calcitonin gene related peptide (CGRP) indicated a significant reduction of positive intraepidermal fibers at the end of treatment (Supplemental Figure1). The morphological and immunohistochemical data are in agreement with the previous findings published in other cisplatin-induced peripheral neuropathy mouse models (13) which identified the main toxic cisplatin action as being in the neuronal DRG somas.

Isolation and Identification of DRG cell populations by single-cell RNA sequencing. To study the intrinsic response of sensory neurons to cisplatin exposure, we performed a single-cell RNA sequencing (scRNAseq) of DRG cells previously isolated by single-cell sorting from control and cisplatin-treated mice (Figure 2, A and B). The analysis was performed one week after the end of cisplatin treatment (10w after the first cisplatin administration). A total of 182 control and 179 cisplatin-treated cells were sequenced. Principal component analysis (PCA) of expression magnitudes across all cells and genes revealed seven distinct cell clusters. These clusters are represented in a t-SNA plot to simplify their visualization (Figure 2C). In order to identify cluster-specific marker genes, the difference in expression of each gene between one cluster and the average in the resting clusters was calculated

(Figure 2D, Supplemental File1). Identification of each cell cluster was then determined by comparing the cluster-specific marker genes with the mouse nervous system scRNAseq database published by Linnarsson Lab (Linnarsson lab Mouse Brain Atlas, RRID:SCR_016999). The different cell clusters were compatible with corresponding to satellite glia cells, glial-like cells, neurons, endothelial/pericytes, perivascular macrophages and vascular smooth muscle cells. The identity of one of the clusters was unclear, presenting mixed markers for different cell types, and therefore it was noted as undefined. Overlaying cells in the t-SNA plot with classical markers for neurons (*Tubb3, Eno2*) (19) and satellite glial cells (*Cdh19, Fabp7*) (20,21) corroborate the identity of these two main cell populations of the DRG cells (Figure 2, E-H).

Cisplatin treatment induces up-regulation of *Cdkn1a* transcription DRG primary neurons. Once the neuronal population was identified, the mRNA transcriptome profiles of 15 control and 43 cisplatin-treated sensory neurons were compared. A total of 122 differentially expressed genes (DEG; $p<0.05$) were detected between both experimental conditions (Supplemental File2). Gene Ontology (GO) analysis of DEG with $p<0.01$ revealed that most of the biological processes up-regulated in the cisplatin group are related to DNA integrity checkpoints as well as DNA damage responses (Supplemental File3). However, to reduce the risk of false significant results after multiple comparisons, p values were corrected and adjusted using the False Discovery Rate (FDR) method, known as p-adjusted-val (p-adj-val) (22). In our experiment, among all the 122 DEG only the *Cdkn1a* gene had a p-adj-val minor than 0.05, so it was considered as a reliable DEG between control and cisplatin conditions (p-adj-val=0.0018; log_FC=0.99) (Supplemental file 2).

To corroborate this significant finding, we first performed a western blot analysis of whole DRG lysates from control and cisplatin-treated animals to check the levels of p21 protein,

which is the product of the *Cdkn1a* gene. We observed a progressive increase of p21 protein levels during the assessment (Figure 3A). In addition, we wanted to identify the specific cell type where p21 was over-expressed. Immunofluorescene (IF) analysis of DRG cross sections also revealed an increase of neuronal nuclei positive for p21 immunoreactivity in the cisplatin group, which reached statistical significance at 16w (Figure 3B).

P21: apoptosis vs senescence pathways. According to our scRNAseq results, p21 emerges as the most relevant downstream checkpoint of the cisplatin-induced DNA damage response in DRG sensory neurons. However, in non-quiescent cells, p21 can be involved in two different and opposite adaptative cellular responses to stressors: apoptosis and senescence (23). Up until now, apoptosis has been extensively described as the main molecular mechanism underlying cisplatin neurotoxicity (14,24,25). To study the activation of apoptosis in our animal model, we checked the levels of cleaved caspase-3, which is necessary for apoptosis execution (26). Western blot analysis in the whole DRG showed that there was no active fragment of caspase-3 (15-17Kda) in any of the time points evaluated in mice treated with cisplatin (Figure 3A). Moreover, levels of Bcl-2 protein were not different among control and cisplatin groups (Figure 3A). Similarly, no nuclear apoptotic changes were observed (Supplemental Figure2). These data point out that the increased levels of p21 do not lead to apoptosis activation. Therefore, we wondered whether cisplatin could be inducing a senescence-like phenotype in DRG neurons in our animal model.

Cisplatin treatment triggers a senescence-like phenotype in DRG sensory neurons. Senescent cells show a lack of uniform definition and phenotype, especially when talking about postmitotic cells. Thus, a combination of multiple biomarkers and morphological

features have been used to define this anti-apoptotic and non-proliferative cellular state (27,28).

To corroborate the hypothesis of a cisplatin-induced senescence-like phenotype in DRG sensory neurons, we first checked the levels of phosphorylated H2AX protein (p-H2AX). This is an early molecular hallmark of DNA damage that has been linked with the occurrence of cellular senescence and final downstream p21 up regulation (29). By western blot, we observed an up-regulation of this protein in DRG of the cisplatin treated mice starting at 10w of treatment (Figure 3A). IF analysis of DRG slices showed that the increase of p-H2AX protein occurs in neuronal nuclei (Figure 3B).

Another feature of senescent cells is the development of a Senescence-secretory associated phenotype (SASP) that consists of a concerted hyper-secretion of pro-inflammatory factors and extracellular matrix proteases (30,31). Thus, we checked the levels of Nfkb-p65 protein, an important inductor of the SASP phenotype (32). Results of western blot showed that cisplatin induces an up-regulation of the Nfkb-p65 protein at 16w of the study (Figure 3A). We observed a progressive significant expression of Nfkb-p65 protein in the nucleus of DRG neurons by IF analysis in cisplatin-treated mice (Figure 3B).

To further corroborate the senescence-like phenotype in sensory neurons after cisplatin exposure, we performed the senescence-associated β-galactosidase (SA-β–GAL) assay in DRG slices, a widely used molecular marker of cell senescence (33,34). Mice treated with cisplatin showed a significantly higher intensity of the SA-β–GAL staining at 16w compared to controls (Figure 4).

Finally, we evaluated the structural changes that DRG sensory neurons suffered after cisplatin treatment by Transmission Electron microscopy (TEM). In comparison to controls, neurons of cisplatin-treated animals presented larger mitochondria, with frequent

fusion/fission like phenomena. Most of these neurons also presented an enlarged endoplasmic reticulum with autophagosome-like vesicles in the periplasmic membrane space. All these changes were qualitatively more pronounced at 16 than at 10w (Figure 5). In addition, we observed accumulation of lipofuscin granules, another senescence hallmark (35) in the neuronal cytoplasm of cisplatin-treated animals at 16w. These granules were not seen in controls nor in treated animals at 10w (Figure 5).

Discussion

The findings of this study suggest that cisplatin adminsitration induces a senescence-like phenotype in the sensory neurons of the mouse DRG. This cellular process is already activated 10w after the first cisplatin administration, as indicated by the increased levels of *Cdnk1a* gene expression, p-H2AX and a concomitant reduction of sensory nerve potential amplitudes. The senescence-like phenotype progresses and is well established by 16w, when multiple molecular and morphological events were observed in the DRG neurons. At this point in time , even when cisplatin has been withdrawn for 6w, a more marked reduction of the amplitude of nerve action potentials is observed, according to what is know as the coasting effect.

DNA damage can arise from multiple origins, including UV light, ionizing radiation or genotoxic chemicals. Whatever the cause, after DNA damage cells activate a complex and tightly regulated network of signalling pathways that constitute the DNA damage response (DDR) intended to safeguard genome integrity (36). When the DDR cannot deal with this damage, cells undergo apoptosis or activate senescence pathways in order to preserve their function or minimize tissue damage (16). While apoptotic programs are well defined (37), cell senescence is a collective phenotype of multiple effector programs, mostly described in replicative cells (38). In fact, the most accepted starting point definition of cell senescence state is provided by the stress-induced arrest and resistance to mitogenic stimuli (39–41). However, this definition is difficult to fit in the postmitotic differentiated cells. Interestingly, molecular markers and effector pathways resembling the senescence phenotype processes have also been identified in non-replicative cells like Purkinje and cortical brain neurons (29,42). In fact, in the context of the neural tissue, with low or restricted regenerative

capacity in response to cellular insults, predominance of the senescence response seems more adaptive than activation of pro-apoptotic programs. In this study, we have demonstrated that cisplatin treatment induces a senescence-like phenotype in DRG sensory neurons in a well-established animal model of peripheral neuropathy. Since senescence is a collective phenotype of multiple effector programs, the induced senescence-phenotype by cisplatin has been corroborated by using a variety of accepted markers implicated in this response.

scRNAseq of sorted neurons from DRG of cisplatin-treated mice showed an up-regulation of GO terms involved in DNA damage responses and the increased of *Cdkn1a* levels. In fact, *Cdkn1a* was the only significant gene upregulated by cisplatin treatment. The limited amount of genetic changes observed in our model can be explained by the low number of sequenced cells or by the fact that cells were sequenced at early stages of neuropathy instauration. The progressive increased expression of *Cdkn1a* product p21 and the early phosphorylation of H2AX as a fast responder to DNA damage corroborated the initial findings obtained in the scRNAseq analysis. Reinforcing our data, previous studies pointed to platinum-induced inter- and intra-strand DNA crosslink damage as the main cause of platinum neurotoxicity (25,43). Moreover, there were neither cleaved caspase-3 nor nuclear apoptotic morphological changes (44) observed in DRG neurons of cisplatin treated mice, indicating that the DDR did not lead to neuronal death by apoptosis. On the other hand, we have found a preservation of myelinayed nerve fibers in our model, as described by others (45–47), with significant reduction in the amplitude of the compound nerve action potentials. These a seemingly discrepant results are compatible with neuronal survival but with a dysfunctional phenotype.

Most studies regarding cisplatin neurotoxicity are focused on activation of the apoptotic pathway triggered by inefficient DNA repair mechanisms. Evidence from in vitro neuronal cultures demonstrated involvement of apoptosis (14,25) However, the evidence in animal models is scarce or even absent (13,48). It has been well established that the cellular response to DNA insults varies depending on the degree and duration of damage. Mild or low prolonged DNA damage results in increased levels of SMAR1, activation of p21 and the direct transcriptional inhibition of BAX and PUMA (49). In contrast, severe DNA damage induces the sequestration of SMAR1 and the activation of apoptotic programs (50). Therefore, a reliable experimental model that closely mimics the clinical situation, with similar equivalent cumulated dose and clinical features, is crucial to indentify the etiopathogenic mechanisms of this neuropathy, especially when adequate patients sample is not available.

Supporting our results, a previous report on microarray analysis of whole DRG from cisplatin treated rats supports our results, as it also found an increased expression of Cdkn1a and metalloprotease 9 (50). The authors related these changes with apoptosis, although the overexpression of these genes can also be involved in senescence. In addition, our hypothesis of cisplatin-induced senescence-like phenotype was further supported by the activation of other senescent markers, like increased activity of SA-βGAL, a maker of lysosome activity (51) and overexpression of Nfkb-p65, a key factor in SASP induction (32) (52). Nfkb-p65 regulates many cellular processes including proliferation, apoptosis and survival. When inactivated, Nfkb-p65 stays in the cytoplasm by binding to their inhibitor Ikb. After activation, Ikb is degraded through the proteasome pathway and Nfkb-p65 is phosphorylated for its translocation to the nucleus (53). Thus, the localization of p65 into the nucleus is a proxy for Nfkb activation (54).

These molecular features are reinforced by the morphological changes that we have found in DRG sensory neurons of cisplatin-treated mice, also reported to be characteristic of cellular senescence, including mitochondrial disturbances, reticulum enlargements and accumulation of intracytoplasmic granules (27,55).

Most of the senescence markers and the cellular changes observed in our model were more marked 16w after the onset of treatment including 6w withdrawal, while neuropathy continues progressing in what we call the coasting effect, which is widely described in patients (56,57). In contrast, p-H2AX increase was already significant at 10 weeks. Phosphorylation of H2AX in Ser139 is a fast response in front DNA damage (58) that has been involved with the development of senescence (29). Therefore, it is to be expected in a situation of active DNA damage, like the one caused by the presence of cisplatin in the cells.

The senescence-like phenotype that sensory neurons develop as a response to cisplatin-induced DNA damage (demonstrated in this study) helps to fit some of the previous findings reported in other models of cisplatin-induced neuropathy. In addition, it also proposes a new etiopathogenic mechanism of platinum-induced peripheral neuropathy that may lead to new approaches in the prevention or even treatment of this important clinical condition that has seen a lack of relevant advances during past decades.

Materials and methods

Animals. 10-weeks-old female BALB/cAnNCrl (BALB/c) mice (19–22g on arrival at the housing room, Janvier) were used for the study. Animals were housed in a limited access animal facility with *ad libitum* access to water and food. Artificial lighting provided a 24-hour cycle of 12 hours light/12 hours dark (light 8 a.m.–8 p.m.).

Drug and treatment schedule. To induce neuropathy, mice were intraperitoneally (i.p.) injected with cisplatin (Cis-diamminedichloroplatinum II, CDDP; Selleckchem) at a dose of 7mg/kg, once a week, for 2 weeks. After that, mice were i.p. administered with 3.5mg/kg cisplatin once a week for a further 8 weeks. After each administration, mice received a subcutaneous (s.c.) injection of 1ml saline to prevent cisplatin-induced nephrotoxicity. The total cumulative dose (TCD) of cisplatin at the end of the study was 42mg/kg. As control group, mice received an i.p. injection of vehicle (saline solution) once a week for 10w.

Functional tests. Functional tests were performed during all the induction time (from 0 to 9w) and up to 6 weeks after the last dose of cisplatin administration (from 10 to 16w) in order to evaluate the coasting-effect (Fig1a).

General toxicity. The physical condition, behavior and reaction to handling of the mice was evaluated once a week. Body weight was recorded for the assessment of the general toxicity of the cisplatin treatment and for dose adjustment.

Nerve conduction studies (NCS). To assess sensory and motor nerve conduction, the sciatic nerve was stimulated percutaneously through a pair of needle electrodes placed at the

sciatic notch and at the ankle. The compound muscle action potential (CMAP) was recorded by microneedle electrodes placed at the plantar muscle. The sensory nerve action potential (SNAP) was recorded from the fourth toe near the digital nerve. The caudal compound nerve action potential (caudal CNAP) was also recorded by placing a pair of recording needle electrodes at the base of the tail and a couple of stimulating needle electrodes at 3.5cm or at 5cm distally to the recording points, assessing proximal and distal orthodromic sensory conductions respectively. Electrophysiological tests were performed before starting the treatment (baseline) and every two weeks during all the follow-up time.

Algesimetry test. Mechanical allodynia was tested by using an electronic Von Frey test Device (IITC Life Science) at baseline and every three weeks. The mean withdrawal pressure of three applications to the left foot was calculated for each animal, and group means were calculated.

Single-cell RNA-sequencing (scRNAseq). At 10w of the study, 5 control and 5 cisplatin-treated mice were sacrificed, intracardially perfused with Dulbeccos Phosphate Buffered Saline (DPBS) w/o Ca^{2+} and Mg^{2+}(Invitrogen) and their DRG sensory neurons analyzed by scRNAseq technique. Cisplatin-treated mice were not selected at random but by taking into account the results of the NCS. Thus, only those mice that had a decrease >15% in their SNAP or Caudal CNAP were used for the scRNAseq.

Single-cell sorting of the DRG. Harvested DRG were enzymatically dissociated with 10x trypsin (Sigma), collagenase A (Sigma) and DNAse (Roche), for 30 minutes at 37ºC and then exposed to mechanical dissociation with a glass pipette. After complete dissociation, cells

were filtered thorugh a 70µm cell strainer and centrifuged at 500rcg. Cells were incubated for 1 hour at 4ºC with primary antibodies rabbit anti-TrkA (1:200, Abcam), goat anti-TrkB (1:200, R&D systems) and goat anti-TrkC (1:200, R&D Systems), diluted in 200 µl FACS incubation medium (NB-A (Thermo Fisher) supplemented with 6mg/ml glucose, 2mM Glutamine (Sigma) and 5% FBS). After washes, cells were incubated for 45 minutes at room temperature with secondary antibodies Alexa 488-conjugated anti-goat (1:200, Invitrogen) and Alexa 488-conjugated anti-rabbit (1:200, Invitrogen) diluted in 200µl FACS incubation medium. After washes, single-cell sorting of DRG cells was carried out using a FacsAria Fusion sorter (Beckton Dickinson), equipped with the ACDU (Automatic Cell Deposition Unit) option. Just before sorting, cells were labeled with Propidium Iodide (PI, excitation at 561 nm – emission at 610/20nm) to exclude permeabilized cells. Alexa488 was excited with a blue (488nm) laser, and fluorescence collected at 530/30 nm. An unstained control was used to place the gate for the positive events. PI-/TRK+ single-cells were sorted into 96-well plates containing RNase Inhibitor solution (Life technologies). After sorting, plates were centrifuged for 1 minute at 4ºC and stored at -80ºC until their analysis by scRNAseq.

RNA-isolation and library construction. Full-length scRNAseq libraries were prepared using the Smart-seq2 protocol (59) with minor modifications. Reverse transcription was performed using SuperScrpit II (Invitrogen) in the presence of oligo-dT30VN, template-switching oligonucleotides and betaine. The cDNA was amplified using the KAPA Hifi Hotstart ReadyMix (Kappa Biosystems), ISPCR primer and 25 cycles of amplification. Following purification with Agencourt Ampure XP beads (Beckmann Coulter), product size distribution and quantity were assessed on a Bioanalyzer using a High Sensitvity DNA Kit (Agilent Technologies). Two hundred picogram of the amplified cDNA was fragmented using

Nextera® XT (Illumina) and amplified with indexed Nextera® PCR primers. Products were purified twice with Agencourt Ampure XP beads and quantified again using a Bioanalyzer High Sensitivity DNA Kit. Sequencing of Nextera® libraries was carried out on a HSeq2500 (Illumina) to obtain approximately 500,000 paired-end 75 bp reads per cell.

scRNAseq analysis, cell type clustering and transcriptome analysis. scRNAseq data was analyzed using the Seurat pipeline (59) implemented in the R language (60) by the *Seurat* package for single cell analysis. The data was pre-processed using the pre-processing workflow in Seurat. Briefly, after loading the count data into R as a Seurat object, the percentage of mitochondrial (%mit) counts in respect of all the counts per cell was calculated as a quality control measure. Cells with less than 100 total counts and with a %mit > 15% were discarded. Subsequently, count data was normalized using the *"LogTransformation"* method in the package. The 15000 most variable transcripts were kept for downstream analysis. For dimensionality reduction, principal component analysis (PCA) was performed after scaling and centering the data, and a permutation test (*JackStraw()* function in the package) was conducted to determine the number of principal components (PCs) to keep (the final number of PCs was 20). For cluster analysis, a shared nearest neighbor graph was constructed and the number of communities (clusters) identified by optimizing modularity (*FindClusters()* function with *resolution* = 0.6). A total of 7 clusters were obtained. We determined cluster identity (cell type) by computing the conserved transcripts (expressed in 95% of the cells of a given cluster, *FindConservedMarkers()* function) across cells from control and cisplatin animals and using the http://mousebrain.org/ atlas as reference (Linnarsson lab Mouse Brain Atlas, RRID:SCR_016999, (61)) for specific profile cell markers. For visualization purposes, a t-

Distributed Stochastic Neighbor Embedding (tSNE) was conducted over the 20 PCs. The subsequent analysis was performed in the neuronal subset. Differentially expressed genes (DEG) between cells coming from control and cisplatin animals were determined using the "MAST" method from the MAST R package (62)called through the *FindMarkers()* function in Seurat. Gene Ontology (GO) enrichment analysis was conducted using the limma package (63) on upregulated or downregulated (cisplatin vs. control) DEGs with p value ≤ 0.01.

Histological methods. At 10 and 16 weeks, mice from control and cisplatin-treated groups were anaesthetized and intracardially perfused with DPBS w/o Ca^{2+} and Mg^{2+}. Different histological studies were performed to further describe the animal model and to corroborate the data obtained with the scRNAseq. Only animals with a decrease in the amplitudes of SNAP or Caudal CNAP >15% were scarified and used for histological analysis at both time points.

Myelinated axons density. A segment of the sciatic nerve at mid-thigh and the distal part of the tibial nerve at the ankle were removed and fixed in glutaraldehyde-paraformaldehyde (3%:3%) in PB 0.1M. The samples were then post-fixed with 2% osmium tetroxide (Sigma) for 2h, dehydrated in graded concentrations of ethanol and embedded in Eponate 12™ resin (Ted Pella Inc). Semithin sections 0.5µm thick were stained with toluidine blue. To estimate the number of myelinated fibers in the sciatic and tibial nerves, axons were counted in images taken on a light microscope (Olympus BX40) attached to a digital camera (Olympus DP73) at 1000x final magnification by using Image J software (NIH, Bathesda, MA). At least 30% of the nerve cross-section area was analyzed.

Intraepidermal nerve fiber density (IENFD). Distal plantar pads were removed and fixed in 4% paraformaldehyde (PFA) in PBS during 1h and washed in PB with sucrose at 4ºC. Cryotome 60µm thick sections were incubated free floating with primary antibodies rabbit anti-PGP9.5 (1:500, Cederlane) or rabbit anti-CGRP (1:1000, Abcam) diluted in blocking solution overnight at 4ºC. After washes, samples were incubated with secondary antibody Cy3 conjugated anti-rabbit IgG (1:500, Jackson Immuno Research). For staining nuclei, DAPI 0.1mg/ml in PBS was added to the samples for 2 minutes. After dehydratation, samples were mounted in gelatin coated slides and viewed in an epifluorescence microscope (Olympus BX51) using an appropriate filter. Five sections from each sample were used to quantify the mean number and density of nerve fibers present in the epidermis of the paw pads.

Transmission electron microscopy of the DRG. Right L4 DRG were removed and post fixed in glutaraldehyde-paraformaldehyde (3%:3%) in PB 0.1M. Following fixation, DRGs were washed with PB followed by centrifugation at 1.278g for 10 minutes. The supernatant was discarded, and the samples resuspended in 1% paraformaldehyde diluted in PB. After washes, DRGs were postfixed for 2h with 1% osmium tetroxide, followed by four washes with deionized water and sequential dehydration in acetone. Samples were embedded in Eponate 12^{TM} resin and polymerized at 60ºC for 48 hours. Ultrathin sections (70nm thick) were placed on non-coated 200 mesh copper grids and contrasted with conventional uranyl acetate solution and Reynolds lead citrate. Sections were observed with a Joel 1400 transmission electron microscope (Joel Ltd) equipped with a Gatan Ultrascan ES1000 CCD Camera.

DRG immunofluorescence. Other DRG samples were embedded in paraffin. Then, microtome section of 5⌠m thickness were deparaffinized with Xylene (Panreac), dehydrated and washed. Antigen retrieval was performed by incubating samples with pre-boiled citrate buffer for 30 minutes. Samples were then permeabilized and incubated with blocking solution (0.3% Triton-100X in PBS with 10% NDS) for 1 hour at room temperature. After blocking, slices were incubated overnight at 4ºC with primary antibodies: rabbit anti-p21 (1:200, Abcam), rabbit anti H2AX-pSer139 (1:200, Cell Signaling), rabbit anti-Nfkb-p65 (1:200, Cell signaling) and mouse anti-®-III-tubulin (1:500, Hybridoma). After washes, samples were incubated for 2 hours at room temperature with secondary antibodies. For staining nuclei, DAPI 0.1µg/ml was added to slices for 2 minutes at room temperature. Images were taken with an epifluorescence microscope (Nikon ECLIPSE Ni) attached to a digital camera (DS-Ri2) at 1000x final magnification. The same threshold of detection and binarization was applied to all the images. The percentages of nuclei positive for p21, p-H2AX and Nfkb-p65 were analyzed in 80-100 neuronal nuclei for each animal by Image J software.

β-*galactosidase activity assay.* β-galactosidase activity was determined in L4 DRG slices following the protocol instructions of the Senescence-detection Kit (Abcam). Briefly, left L4 DRG were dissected from mice and immediately snap freeze in liquid nitrogen. 15µm-thick cryostat sections were mounted in gelatin-coated slides. Immediately, samples were fixed in the fixative solution for 10 minutes and then washed twice with PBS. Sections were then incubated with the staining solution at 37ºC O.N. Images were taken in a light phase microscope (Nikon ECLIPSE Ni) attached to a digital camera (DS-Ri2) at 400x final magnification chosen by systematic random sampling of squares. The intensity of the β-

galactosidase reaction (seen as a blue precipitate) was quantified in a total of 50 neurons for each animal using Image J software.

Western Blot analysis. All DRGs from lumbar to cervical segments were dissected from DPBS perfused mice and immediately snap frozen in liquid nitrogen. DRGs were then homogenized in modified RIPA lysis buffer adding 10 µl/ml of Protease Inhibitor cocktail (Sigma) and PhosphoSTOP phosphatase inhibitor cocktail (Roche). Protein was quantified by BCA protein assay (Thermo Scientific). 30⌈g of protein from each sample were loaded in 15% SDS-polyacrylamide gels. The transfer was made 1h at room temperature with a constant voltage of 90V. After blockade, membranes were incubated overnight at 4ºC with primary antibodies: anti-p21 (1:200, Abcam), anti H2AX(ser139) (1:1000, Cell Signaling), anti-cleaved caspase 3 (1:500, Cell Signaling), anti-caspase 3 (1:500, Cell Signaling), anti-Nfkb-p65 (1:1000, Cell Signaling), anti-Bcl-2 (1:500 Abcam) and anti-GAPDH (1:10000, Millipore). Horseradish peroxidase-coupled secondary antibody incubation was performed for 90 minutes at room temperature. Membranes were visualized using the enhanced chemiluminescence method with the clarity western ECL substrate (Bio Rad). Images were collected using a chemidoc apparatus. Western blots were then analyzed using the Lane and band plugin form the Image Lab software (Bio Rad). Data were normalized first by the loading control (GAPDH) and afterwards by the mean of the control samples. 4-7 samples were analyzed per each treatment condition and time point of study.

Statistics. The results of functional tests are expressed as a percentage with respect to baseline values for each mouse and statistical analysis were performed by using repeated measures two-way ANOVA test (RM ANOVA). For the other comparisons, one-way ANOVA

test was used. The Bonferroni post hoc test was applied when needed. Graph Pad Prism 8 (Version 8.4.0) software was used to statistical inference analysis and graphically represent the data, which are expressed as Group Mean ±standard deviation. Differences among groups or time points were considered significant at $p<0.05$.

Study approval. All the animal studies were approved by the Ethics Committee of the Universitat Autònoma de Barcelona.

Author contributions

AC conducted the experiments, acquired and analyzed data, and contributed to writing the manuscript. ATE analyzed and interpreted data, and contributed to writing the manuscript. XN and VY provided reagents, contributed to interpreting data and writing the manuscript. EU designed the study, interpreted data and contributed to writing the manuscript. JB designed the study, conducted experiments, interpreted data and contributed to writing the manuscript.

Acknowledgments

The authors research was supported by funds from CIBERNED and TERCEL networks to XN, and by a PI1501303 grant to JB from the Instituto de Salud Carlos III of Spain, co-funded by European Union (ERDF/ESF, “Inesting in yout future”). JB has received support from grant number SLT008/18/00028 from the Department of Health of the Government of Catalonia, CERCA Program. AC was recipient of a predoctoral fellowship from the Secretaria d’Universitats i Recerca of the Catalan Government (FI fellowship). The authors thank the technical support of Monica Espejo, Jessica Jaramillo and Mar del Castillo from the Institute of Neuroscience and Alex Sánchez from the Microscopy Service of the Universitat Autònoma de Barcelona. Authors also thank Jaume Comas from the cytometry and genomics service of the CCit UB and Holger Heyn and Catia Moutinho from the Centro nacional de anàlisis genòmica (CNAG).

References

1. Argyriou AA, Bruna J, Marmiroli P, Cavaletti G. Chemotherapy-induced peripheral neurotoxicity (CIPN): An update. Crit Rev Oncol Hematol. 2012; 82(1): 51-77.
2. Jagannath S, Barlogie B, Berenson JR, Siegel DS, Irwin D, Richardson PG, et al. Updated survival analyses after prolonged follow-up of the phase 2, multicenter CREST study of bortezomib in relapsed or refractory multiple myeloma. Br J Haematol. 2008; 143(4): 537-40.
3. Lee J chan, Kim JW, Ahn S, Kim HW, Lee J, Kim YH, et al. Optimal dose reduction of FOLFIRINOX for preserving tumour response in advanced pancreatic cancer: Using cumulative relative dose intensity. Eur J Cancer. 2017; 76: 125-133.
4. Mols F, Beijers T, Lemmens V, Van Den Hurk CJ, Vreugdenhil G, Van De Poll-Franse L V. Chemotherapy-induced neuropathy and its association with quality of life among 2- to 11-year colorectal cancer survivors: Results from the population-based PROFILES registry. J Clin Oncol. 2013; 31(21): 2699-707.
5. Pike CT, Birnbaum HG, Muehlenbein CE, Pohl GM, Natale RB. Healthcare Costs and Workloss Burden of Patients with Chemotherapy-Associated Peripheral Neuropathy in Breast, Ovarian, Head and Neck, and Nonsmall Cell Lung Cancer. Chemother Res Pract. 2012; 2012: 913848.
6. Yarchoan M, Johnson BA, Lutz ER, Laheru DA, Jaffee EM. Targeting neoantigens to augment antitumour immunity. Nat Rev Cancer. 2017. 17(9): 569.
7. Chu E, DeVita Jr. VT. Physicians' Cancer Chemotherapy Drug Manual 2019. 19th edition. Massachusetts: Jones and Bartlett Publishers; 2019.
8. Staff NP, Cavaletti G, Islam B, Lustberg M, Psimaras D, Tamburin S. Platinum-induced peripheral neurotoxicity: From pathogenesis to treatment. J Peripher Nerv

Syst. 2019; Suppl 2: S26-S39.

9. Albers JW, Chaudhry V, Cavaletti G, Donehower RC. Interventions for preventing neuropathy caused by cisplatin and related compounds. Cochrane Database Syst Rev. 2014; (3): CD005228.

10. Hershman DL, Lacchetti C, Dworkin RH, Lavoie Smith EM, Bleeker J, Cavaletti G, et al. Prevention and management of chemotherapy-induced peripheral neuropathy in survivors of adult cancers: American society of clinical oncology clinical practice guideline. J Oncol Pract. 2014; 10(6): e421-e424.

11. Ghosh S. Cisplatin: The first metal based anticancer drug. Bioorg Chem. 2019; 88:102925.

12. Gregg RW, Molepo JM, Monpetit VJA, Mikael NZ, Redmond D, Gadia M, et al. Cisplatin neurotoxicity: The relationship between dosage, time, and platinum concentration in neurologic tissues, and morphologic evidence of toxicity. J Clin Oncol. 1992; 10(5): 795-803.

13. Calls A, Carozzi V, Navarro X, Monza L, Bruna J. Pathogenesis of platinum-induced peripheral neurotoxicity: Insights from preclinical studies. Exp Neurol. 2020; 325: 113141.

14. Gill JS, Windebank AJ. Cisplatin-induced apoptosis in rat dorsal root ganglion neurons is associated with attempted entry into the cell cycle. J Clin Invest. 1998; 101(12): 2842-50.

15. Manu KA, Cao PHA, Chai TF, Casey PJ, Wang M. p21cip1/waf1 Coordinate Autophagy, Proliferation and Apoptosis in Response to Metabolic Stress. Cancers (Basel). 2019;11(8):1112.

16. Fielder E, Von Zglinicki T, Jurk D. The DNA Damage Response in Neurons: Die by Apoptosis or Survive in a Senescence-Like State? J Alzheimers Dis. 2017; 60(s1):

S107-S131.

17. Reagan-Shaw S, Nihal M, Ahmad N. Dose translation from animal to human studies revisited. FASEB J. 2008; 22(3): 659-61.

18. Krarup-Hansen A, Helweg-Larsen S, Schmalbruch H, Rørth M, Krarup C. Neuronal involvement in cisplatin neuropathy: Prospective clinical and neurophysiological studies. Brain. 2007; 130(Pt4): 1076-88.

19. Usoskin D, Furlan A, Islam S, Abdo H, Lönnerberg P, Lou D, et al. Unbiased classification of sensory neuron types by large-scale single-cell RNA sequencing. Nat Neurosci. 2015; 18(1): 145-53.

20. Avraham O, Deng P-Y, Jones S, Kuruvilla R, Semenkovich CS, Klyachko VA, et al. Fatty acid synthesis in satellite glial cell promotes regenerative growth in sensory neurons. bioRxiv. 2019.

21. George D, Ahrens P, Lambert S. Satellite glial cells represent a population of developmentally arrested Schwann cells. Glia. 2018; 66(7): 1496-1506.

22. Benjamini Y, Hochberg Y. Controlling the False Discovery Rate: A Practical and Powerful Approach to Multiple Testing. J R Stat Soc Ser B. 1995; 57(1): 289-300.

23. Kreis NN, Louwen F, Yuan J. The multifaceted p21 (Cip1/Waf1/CDKN1A) in cell differentiation, migration and cancer therapy. Cancers (Basel). 2019; 11(9): 1220.

24. Alaedini A, Xiang Z, Kim H, Sung YJ, Latov N. Up-regulation of apoptosis and regeneration genes in the dorsal root ganglia during cisplatin treatment. Exp Neurol. 2008; 210(2): 368-74.

25. McDonald ES, Randon KR, Knight A, Windebank AJ. Cisplatin preferentially binds to DNA in dorsal root ganglion neurons in vitro and in vivo: A potential mechanism for neurotoxicity. Neurobiol Dis. 2005; 18(2): 305-13.

26. McIlwain DR, Berger T, Mak TW. Caspase functions in cell death and disease. Cold

Spring Harb Perspect Biol. 2013; 5(4): a008656.

27. Martínez-Zamudio RI, Robinson L, Roux PF, Bischof O. SnapShot: Cellular Senescence Pathways. Cell. 2017. 170(4): 816.

28. Rodier F, Campisi J. Four faces of cellular senescence. J Cell Biol. 2011; 192(4): 547-56.

29. Jurk D, Wang C, Miwa S, Maddick M, Korolchuk V, Tsolou A, et al. Postmitotic neurons develop a p21-dependent senescence-like phenotype driven by a DNA damage response. Aging Cell. 2012; 11(6): 996-1004.

30. Basisty N, Kale A, Jeon OH, Kuehnemann C, Payne T, Rao C, et al. A proteomic atlas of senescence-associated secretomes for aging biomarker development. PLoS Biol. 2020; 18(1): e30000599.

31. Rodier F, Coppé JP, Patil CK, Hoeijmakers WAM, Muñoz DP, Raza SR, et al. Persistent DNA damage signalling triggers senescence-associated inflammatory cytokine secretion. Nat Cell Biol. 2009; 11(8): 973-9.

32. Chien Y, Scuoppo C, Wang X, Fang X, Balgley B, Bolden JE, et al. Control of the senescence-associated secretory phenotype by NF-κB promotes senescence and enhances chemosensitivity. Genes Dev. 2011; 25(20): 2125-36.

33. Dimri GP, Lee X, Basile G, Acosta M, Scott G, Roskelley C, et al. A biomarker that identifies senescent human cells in culture and in aging skin in vivo. Proc Natl Acad Sci U S A. 1995; 92(20): 9363-7.

34. Tominaga T, Shimada R, Okada Y, Kawamata T, Kibayashi K. Senescence-associated-β-galactosidase staining following traumatic brain injury in the mouse cerebrum. PLoS One. 2019; 14(3): e0213673.

35. Georgakopoulou EA, Tsimaratou K, Evangelou K, Fernandez-Marcos PJ, Zoumpourlis V, Trougakos IP, et al. Specific lipofuscin staining as a novel

biomarker to detect replicative and stress-induced senescence. A method applicable in cryo-preserved and archival tissues. Aging (Albany NY). 2013; 5(1): 37-50.

36. Jackson SP, Bartek J. The DNA-damage response in human biology and disease. Nature. 2009. 461(7267): 1071-8.

37. D'Arcy MS. Cell death: a review of the major forms of apoptosis, necrosis and autophagy. Cell Biol Int. 2019; 43(6): 582-592.

38. Hernandez-Segura A, Nehme J, Demaria M. Hallmarks of Cellular Senescence. Trends Cell Biol. 2018; 28(6): 436-453.

39. Campisi J, D'Adda Di Fagagna F. Cellular senescence: When bad things happen to good cells. Nat Rev Mol Cell Biol. 2007; 8(9): 729-40.

40. Salama R, Sadaie M, Hoare M, Narita M. Cellular senescence and its effector programs. Genes Dev. 2014; 28(2): 99-114.

41. Sharpless NE, Sherr CJ. Forging a signature of in vivo senescence. Nat Rev Cancer. 2015; 15(7): 397-408.

42. Geng YQ, Guan JT, Xu XH, Fu YC. Senescence-associated beta-galactosidase activity expression in aging hippocampal neurons. Biochem Biophys Res Commun. 2010; 396(4): 866-9.

43. Ta LE, Espeset L, Podratz J, Windebank AJ. Neurotoxicity of oxaliplatin and cisplatin for dorsal root ganglion neurons correlates with platinum-DNA binding. Neurotoxicology. 2006; 27(6): 992-1002.

44. Martelli AM, Zweyer M, Ochs RL, Tazzari PL, Tabellini G, Narducci P, et al. Nuclear apoptotic changes: An overview. J Cell Biochem. 2001; 82(4): 634-46.

45. Carozzi VA, Canta A, Oggioni N, Sala B, Chiorazzi A, Meregalli C, et al. Neurophysiological and neuropathological characterization of new murine models of chemotherapy-induced chronic peripheral neuropathies. Exp Neurol. 2010; 226(2):

301-9.

46. Carozzi VA, Chiorazzi A, Canta A, Meregalli C, Oggioni N, Cavaletti G, et al. Chemotherapy-induced peripheral neurotoxicity in immune-deficient mice: New useful ready-to-use animal models. Exp Neurol. 2015;264:92–102.

47. Verdú E, Vilches JJ, Rodríguez FJ, Ceballos D, Valero A, Navarro X. Physiological and immunohistochemical characterization of cisplatin- induced neuropathy in mice. Muscle Nerve. 1999; 22(3): 329-40.

48. Fischer SJ, McDonald ES, Gross LA, Windebank AJ. Alterations in cell cycle regulation underlie cisplatin induced apoptosis of dorsal root ganglion neurons in vivo. Neurobiol Dis. 2001; 8(6): 1027-35.

49. Sinha S, Malonia SK, Mittal SPK, Singh K, Kadreppa S, Kamat R, et al. Coordinated regulation of p53 apoptotic targets BAX and PUMA by SMAR1 through an identical MAR element. EMBO J. 2010; 29(4): 830-42.

50. Jalota A, Singh K, Pavithra L, Kaul-Ghanekar R, Jameel S, Chattopadhyay S. Tumor suppressor SMAR1 activates and stabilizes p53 through its arginine-serine-rich motif. J Biol Chem. 2005; 280(16): 16019-29.

51. Lee BY, Han JA, Im JS, Morrone A, Johung K, Goodwin EC, et al. Senescence-associated β-galactosidase is lysosomal β-galactosidase. Aging Cell. 2006; 5(2): 187-95.

52. Lopes-Paciencia S, Saint-Germain E, Rowell MC, Ruiz AF, Kalegari P, Ferbeyre G. The senescence-associated secretory phenotype and its regulation. Cytokine. 2019; 117: 15-22.

53. Wan F, Lenardo MJ. The nuclear signaling of NF-κB: Current knowledge, new insights, and future perspectives. Cell Res. 2010; 20(1): 24-33.

54. Maguire O, Collins C, O'Loughlin K, Miecznikowski J, Minderman H. Quantifying

nuclear p65 as a parameter for NF-κB activation: Correlation between ImageStream cytometry, microscopy, and Western blot. Cytometry A. 2011; 79(6): 461-9.

55. Denoyelle C, Abou-Rjaily G, Bezrookove V, Verhaegen M, Johnson TM, Fullen DR, et al. Anti-oncogenic role of the endoplasmic reticulum differentially activated by mutations in the MAPK pathway. Nat Cell Biol. 2006; 8(10): 1053-63.

56. Brouwers EEM, Huitema ADR, Boogerd W, Beijnen JH, Schellens JHM. Persistent neuropathy after treatment with cisplatin and oxaliplatin. Acta Oncol. 2009; 48(6): 832-41.

57. Pietrangeli A, Leandri M, Terzoli E, Jandolo B, Garufi C. Persistence of high-dose oxaliplatin-induced neuropathy at long-term follow-up. Eur Neurol. 2006; 56(1): 13-6.

58. Sharma A, Singh K, Almasan A. Histone H2AX phosphorylation: A marker for DNA damage. Methods Mol Biol. 2012; 920: 613-26.

59. Picelli S, Björklund ÅK, Faridani OR, Sagasser S, Winberg G, Sandberg R. Smart-seq2 for sensitive full-length transcriptome profiling in single cells. Nat Methods. 2013; 10(11): 1096-8.

60. R Development Core Team R. R: A Language and Environment for Statistical Computing. R Foundation for Statistical Computing. 2011.

61. Zeisel A, Hochgerner H, Lönnerberg P, Johnsson A, Memic F, van der Zwan J, et al. Molecular Architecture of the Mouse Nervous System. Cell. 2018; 174(4): 999-1014.

62. Finak G, McDavid A, Yajima M, Deng J, Gersuk V, Shalek AK, et al. MAST: A flexible statistical framework for assessing transcriptional changes and characterizing heterogeneity in single-cell RNA sequencing data. Genome Biol. 2015; 16: 278.

63. Ritchie ME, Phipson B, Wu D, Hu Y, Law CW, Shi W, et al. Limma powers differential expression analyses for RNA-sequencing and microarray studies. Nucleic Acids Res. 2015; 43(7): 47.

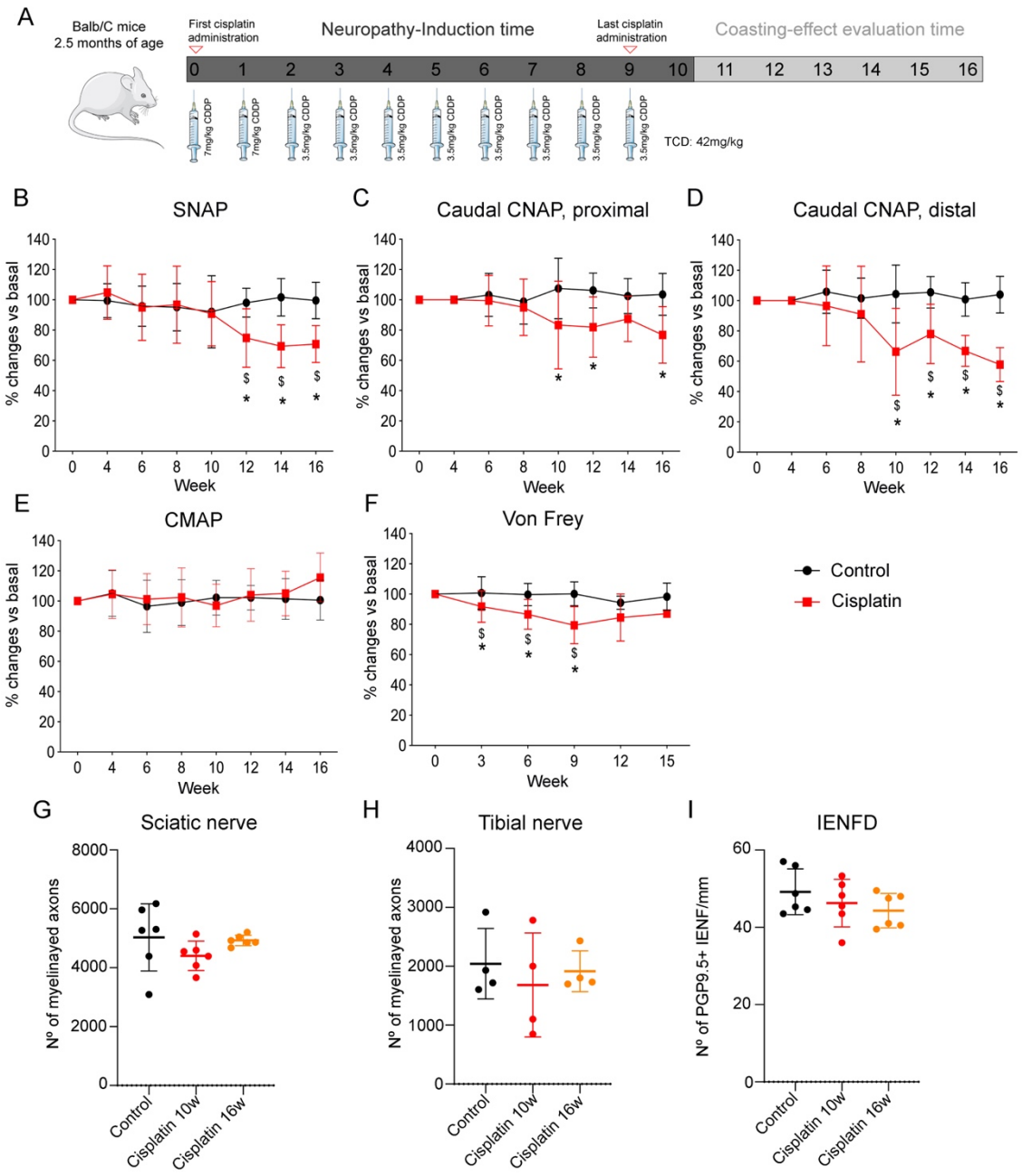

Figure 1. Functional and histological characterization of the Cisplatin-induced peripheral neuropathy mouse model. A: Timeline representing the development of the cisplatin induced peripheral neuropathy model. Cisplatin was administered i.p. once a week for 10w (Neuropathy-induction time). The total cumulated dose (TCD) at the end of the induction time was 42mg/kg. After this time, animals were still evaluated to assess the coasting effect (coasting-effect evaluation time). B-E: Nerve conduction studies (n=20-25 mice/group). Nerve conduction resuts from recordings in the sensory digital nerve (B), the proximal and distal caudal nerve (C-D) and the plantar muscle (E) show a reduction in the amplitudes of the compound sensory nerve action potentials (SNAP, Caudal CNAP) but not in the compound motor action potential (CMAP). F: Mice treated with cisplatin developed mechanical allodynia until week 9. After that, the withdrawal threshold to mechanical

stimulus tended to recover to basal values (n=25 mice/group). G-I: Histological results. Cisplatin did not induce a significant reduction in the total number of myelinated axons of the sciatic nerve (n=6 mice/group) (G) nor in the tibial nerve (n=4 mice/group) (H). Cisplatin did not cause a reduction of the number of PGP9.5+ intraepidermal nerve fibers in the plantar pad of the mice (n=6 mice/group) (I). Repeated measures ANOVA test for functional studies. One Way ANOVA test for histological studies. Bonferroni post-hoc test was used for mutliple comparisons. *$p<0.05$ vs control; \$$p<0.05$ vs basal values (time effect). Data is represented as Group Mean±SD.

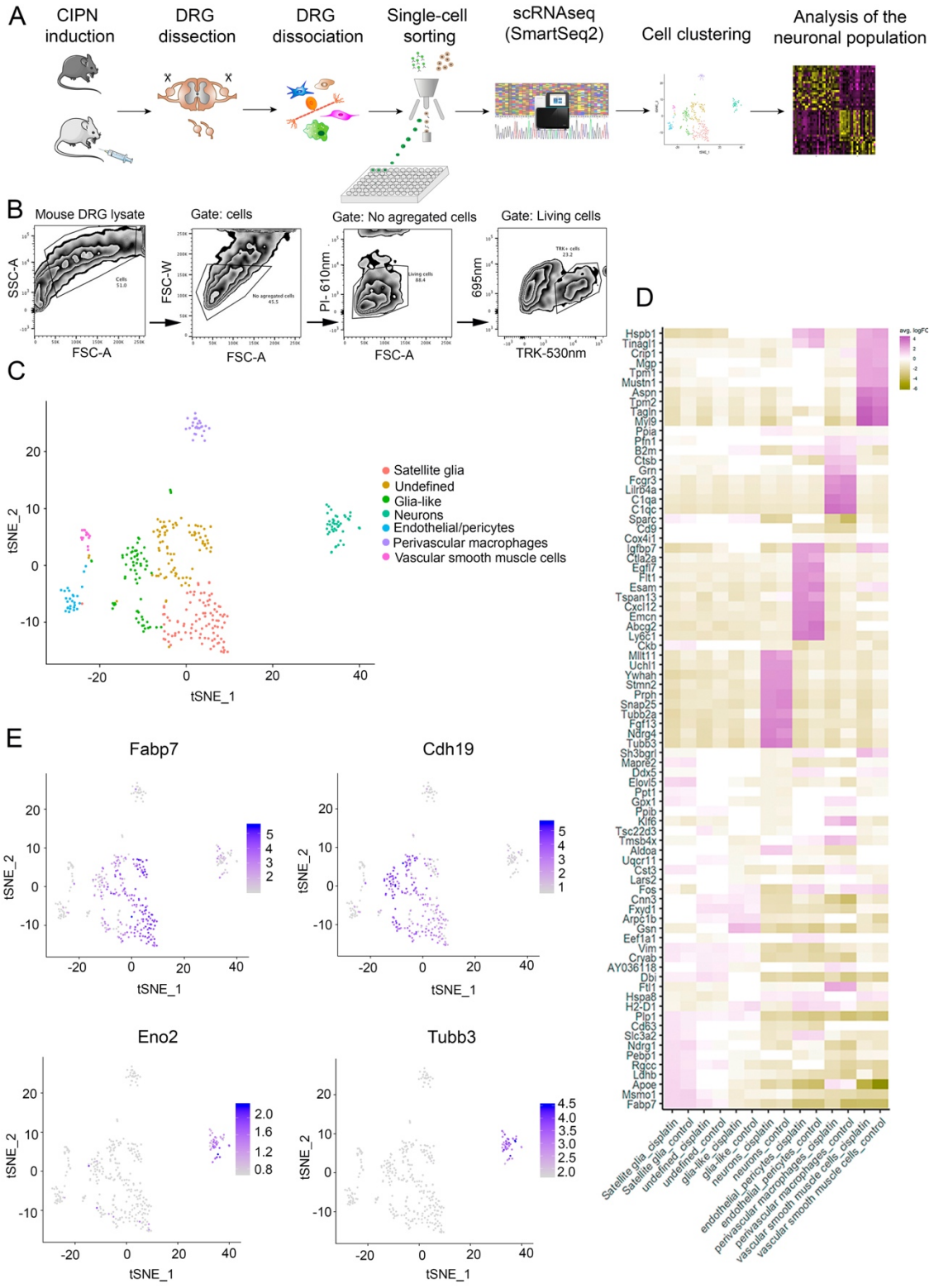

Figure 2. Specific DRG cell populations were obtained by single-cell RNA-sequencing with previous cell isolation by single-cell sorting. A: Schematic representation of the experimental design followed in this study. After induction of cisplatin neuropathy, control and treated mice were sacrified and their DRGs were dissected and enzymatically dissociated. Individual DRG cells were isolated in 96-well plates by single-cell sorting. Each

sorted cell was then sequenced by scRNAseq (smartSeq2). Cell type populations were defined by checking the expression of well established cellular markers. Finally, differences between the transcriptome of control and cisplatin-treated neurons were analyzed. B: Plots showing the process followed to isolate DRG cells by single cell sorting. The cell population was selected according to size (FSC-A/SSC-A) and aggregated cells were discarded to ensure the single-cell sorting (FSC-A/FSC-W). Then, death cells were excluded by gating the cells without Propidium iodide immunoreactivity (PI). Finally, only living cells expressing TRK were collected. C: t-SNA plot representing the data of the PCA analysis of mRNA transcriptome in the individual sorted DRG cells (each point refers to an individual cell). Cells were tagged for a specific cell type according to their different expression patterns of marker genes. D: Heat map showing the Top 10 genes defining each cellular cluster. Unique cell clusters were not altered by cisplatin treatment. E: Relative expression level of DRG satellite glia (C*dh19* and *Fabp7*) and sensory neurons (*Tubb3* and *Eno2*) markers are mapped to each cell in the t-SNA plot. Color key represents normalized gene expression with the highest expression marked purple and the lowest marked gray.

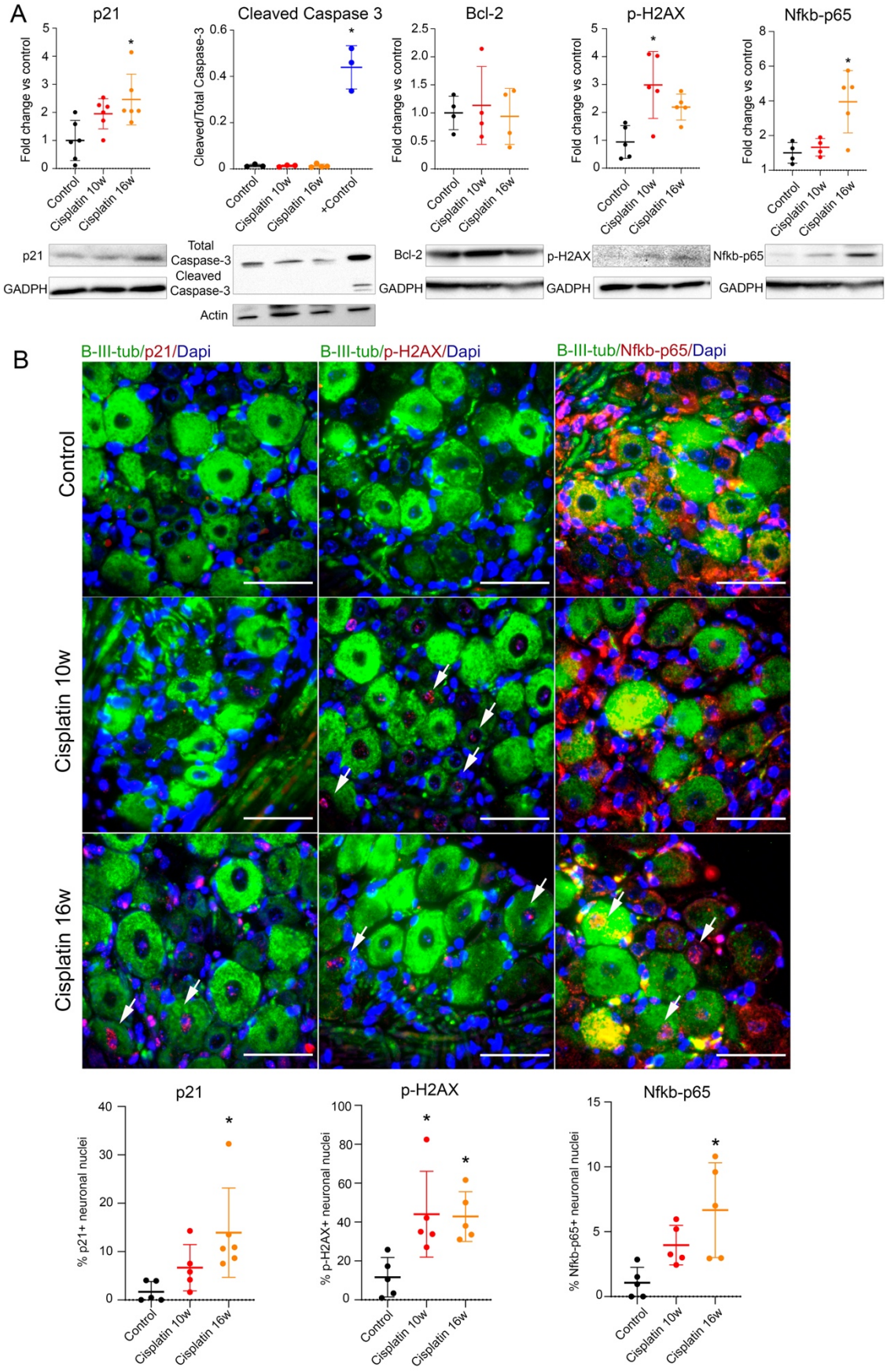

Figure 3. Cisplatin treatment induces molecular senescence hallmarks in DRG neurons from mice without evidence of apoptosis induction. A: Western Blot analysis of whole

lysate DRG in control and cisplatin-treated mice show an increase in the expression of p21, p-H2AX and Nfkb-p65 proteins in the cisplatin-treated group. No active (cleaved) caspase-3 is present in the treated group at any of the time points evaluated. Similarly, no differences in Bcl-2 protein levels are observed among control and treated groups. Up: Barr graphs representing the quantification of each protein analyzed. Below: representative blots of the corresponding protein. +Control refers to SH-ST5Y cells treated with 1µM staurosporine for 6 hours. (n= 3-5 mice/group). B: Immunofluorescence analysis of p21, p-H2AX and Nfkb-p65 proteins in DRG reveals that these proteins are expressed in neuronal nuclei after cisplatin administration. Up: Representative images of p21 (left), p-H2AX (medium) and Nfkb-p65 (right) immunofluorescence (in red) in the DRG of control and cisplatin-treated mice. Neurons were stained with the pan-neuronal marker ß-III-tubulin (green) and nuclei were counterstained with dapi (blue). White arrows show neuronal nuclei positive for p21, p-H2AX or Nfkb-p65. Down: bar graphs representing the percentage of neuronal nuclei positive for p21 (right), p-H2AX (medium) and Nfkb-p65 (left) proteins from the total neuronal nuclei. Around 100 nuclei were quantified per each animal and protein of interest. (n=5-6 mice/group). Scale: 50µm. One Way ANOVA test. Bonferroni post-hoc test was used for multiple comparisons. *$p<0.05$ vs Control group. Data is represented as Group Mean± SD.

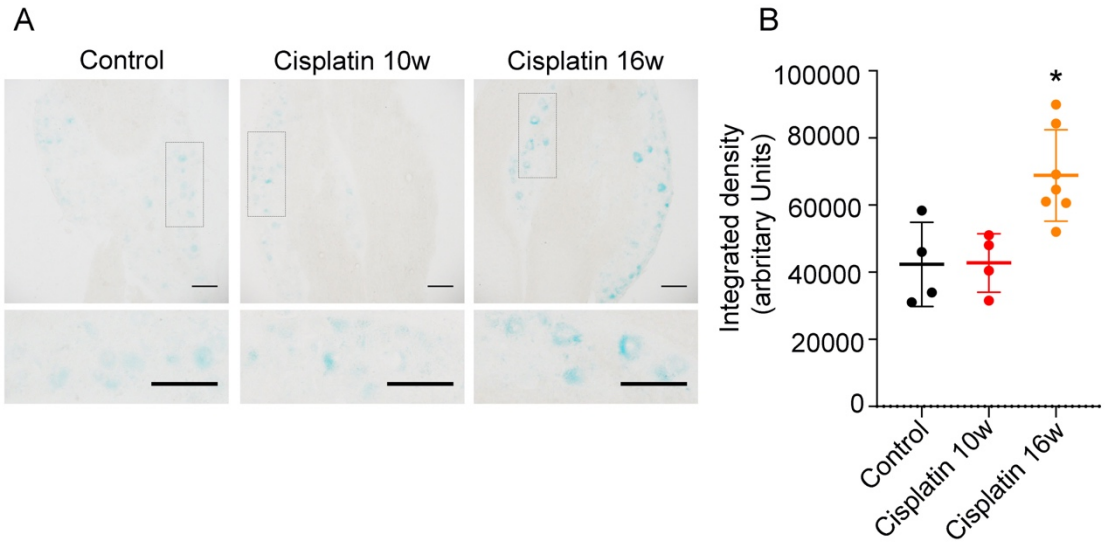

Figure 4. Senescence associated β-galactosidase (SA-β-GAL) staining in DRG of control and cisplatin-treated mice. A: SA-β-gal positive neurons are seen in DRG of control and cisplatin-treated mice at 10w and 16w of study. Images below correspond to a magnification of the box-delimited areas of the upper images. Scale: 100µm. B: Graph Bars showing the quantification of the SA-β-GAL staining intensity in control and cisplatin treated mice (n=4-7 mice/group). One Way ANOVA test. Bonferroni post-hoc test was used for mutliple comparisons. *p<0.05. Data is represented as Group Mean± SD

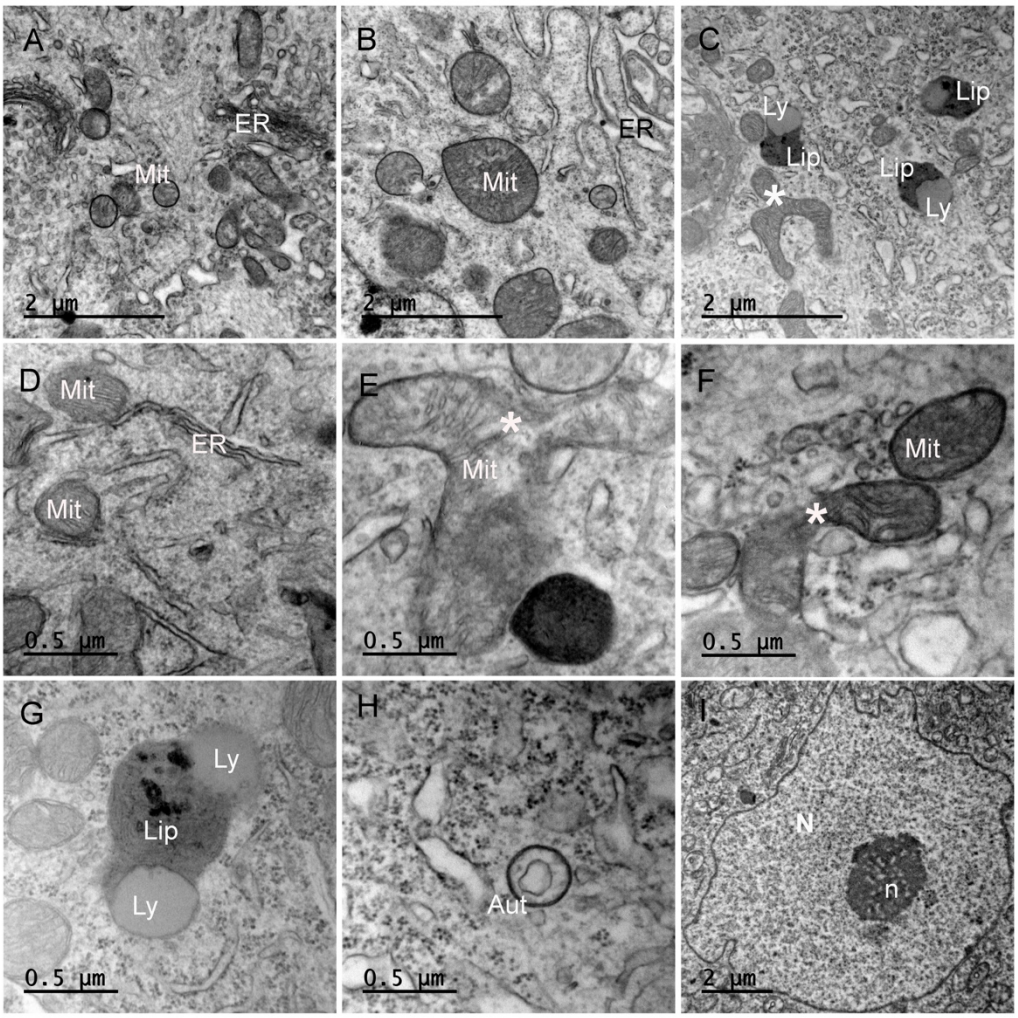

Figure 5. Representative TEM images of DRG neurons from control (A, D) and cisplatin-treated mice at 10w (B, E) and 16w (C, F-I). A-C: General view of the neuronal cytoplasm of control (A) and cisplatin-treated mice at 10w (B) and 16w (C). Mitochondria (Mit) and endoplasmic reticulum (ER) appear dilated in cisplatin-treated animals at both 10w and 16w when compared with control. Moreover, at 16w, neurons from the cisplatin condition present lysosome vesicles (Ly) and lipofuscin granules (Lip). D-I: magnified views of the neuronal cytoplasm of control (D) and cisplatin-treated mice (E-I). In the cisplatin conditions, it is frequent to see fission/fusion mitochondrial phenomena (E-F), which are rare in the control condition. Fission/fusion mitochondria phenomena are indicated with an asterisk (*). Lipofuscin granules (Lip), lysosomes vesicles and Autophagosome-like vesicles (Aut) are seen in DRG sensory neurons from cisplatin-treated mice at 16w. At these timepoint, neuronal nuclei (N) have normal morphology with no alterations in the nucleoli (n) nor in the chromatin.

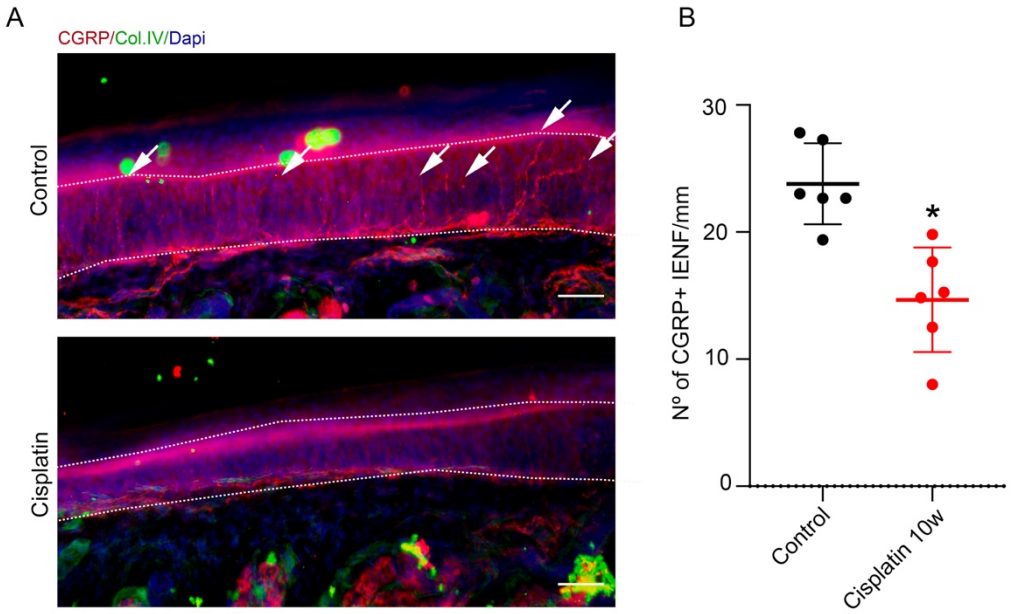

Supplemental Figure 1. Cisplatin treatment induces a reduction of the IENFD of CGRP+ fibers at 10w. A: Representative images of the epidermis immunolabeled against CGRP (red) in the pad paw from control (up) and cisplatin-treated mice at 10w (bottom). To localize the epidermis (area inside the white boxes), immunoreactivity against Collagen IV (green) was used. DAPI (blue) was applied to constrain nuclei. White arrows indicate CGRP+ nerve fibers. Scale: 50µm. B: graph bar with the quantification of the IENFD of CGRP+ fibers in mice epidermis (n=6 mice/group). Unpaired T-student test.*p<0.05 vs CONTROL. Data is represented as Group Mean± SD.

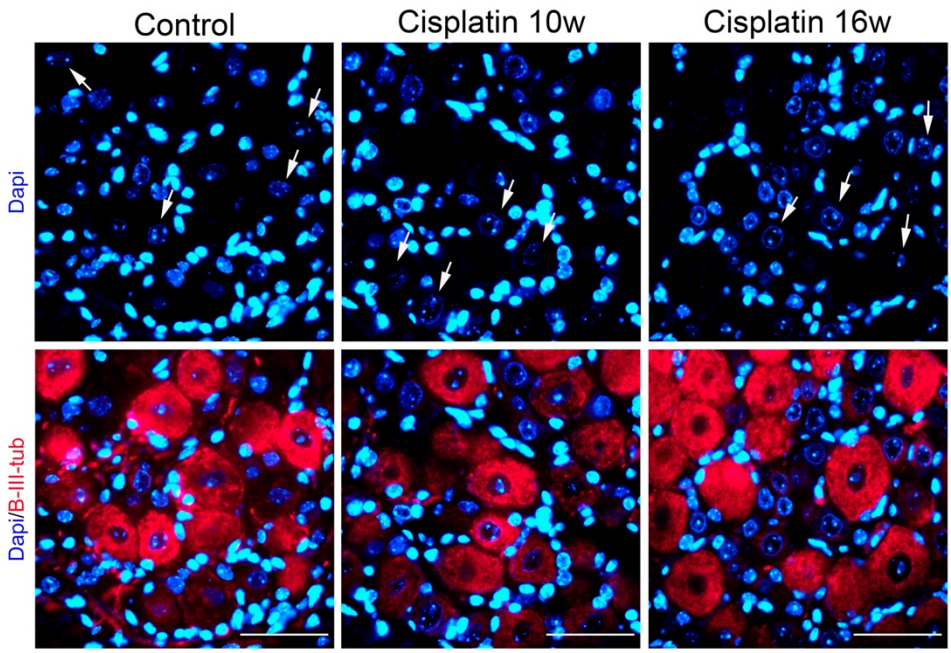

Supplemental Figure 2. No apoptotic nuclei in sensory neurons of DRG from cisplatin treated mice. Images of nuclei from DRG slices stained with Dapi (blue) and B-III-tubulin (red). Neither sensory neurons nor other cell types present in the DRG of treated mice show morphological signs of apoptosis in their nuclei at 10w and 16w follow up. White arrows indicate neuronal nuclei. Scale: 50µm.